Open Circuit Potential (OCP) as a tool for the assessment of binding kinetics and reagentless protein quantitation

Mohamed Sharafeldin;[1] Timothy James;[2] and Jason J. Davis*[1]

[1] Department of Chemistry, University of Oxford, South Parks Road, Oxford OX1 3QZ, UK

[2] Department of Clinical Biochemistry, Oxford University Hospitals NHS Trust, Oxford, OX3 9DU, U.K.

***KEYWORDS**: Open Circuit Potential; Microfluidics; Binding kinetics; Protein quantification; Reagentless; Diagnostics*

Corresponding Author email: Jason.Davis@chem.ox.ac.uk

ABSTRACT: A microfluidic open circuit potential (OCP) label-free protein assay was developed for the reagentless quantification of C-reactive protein (CRP), a model protein target, and further utilized to assess target-receptor binding kinetics. Generated sensors have very high baseline stabilities (<1% change in 100 minutes) and high levels of selectivity in complex media. Real-time assays are fast (<20 minutes), of high sensitivity (1 ng/mL limit of detection (LOD) of CRP in serum) and resolve kinetic and thermodynamic characteristics that correlate well with those resolved optically. The assay shows excellent correlation with an ELISA analysis of patient samples. The methodology has value in potentially underpinning a low-cost, rapid and sensitive single step biomarker quantification.

Introduction

A quantitation of protein markers, and any assessment of their specific binding affinities, lies central to much of diagnostics, drug development and immunotherapy. Quantification from complex media, with associated cross reference to projected symptoms and metabolic status, has offered insight into disease progression, diagnosis, and clinical assessments of treatment plans.[1] It has, additionally, been of substantial value in improving our understanding and intervention of cancers,[2] neurological disorders,[3] cardiovascular diseases[4,5] and many pathogenic infections.[6] Kinetic analyses underpin developments in immunotherapeutics,[7] drug discovery,[8,9] development and validation of antibodies.[10] A number of physical methods are able to input into such (quantification or kinetic) assessments. These include the enzyme-linked immunosorbent assay (ELISA),[11,12] surface plasmon resonance (SPR),[13] electrophoresis,[14] mass spectrometry (MS),[15] calorimetry,[16] and bio-layer interferometry.[17] Though ELISA, MS and SPR in particular constitute laboratory workhorses, there are well-established issues associated with hardware cost and/or exhaustive multi-step protocols.[18,19]

A miniaturization of this capability not only puts such analyses in the hands of many more personnel (including those at a point of care) but also often enables such with greater brevity and

lower sample volume.[20] Electrochemical/electrical methods, in particular, are natively highly scaleable in this sense (in terms of fabrication cost, portability and flexible device integration).[21–24] Although a number of potent electrochemical formats have been reported at depth, many require a pre-labelling of receptors or the use of secondary amplification effects, and few have offered any assessment of protein binding kinetics. Solid-state resistive pulse nanopores have recently been proposed here but suffer from high background noise, and require both specifically engineered proteins and demanding pore assembly.[25–27] Amperometric aptamer based assays are potentially reagentless, operate without a need for amplification, and able to report on binding dynamics (albeit for a limited number of targets to date).[28] They operate, however, on substantial binding-induced nucleic acid conformational change in specifically engineered receptors, and cannot be applied to any direct assessment of protein: protein interaction.[29,30] Impedimetric assays can offer high levels of sensitivity but typically require the pre-doping of analytical solutions with a large excess of amplifying redox probe.[31] Alternatively, the integration of redox capacitative elements into a receptive interface can also lead to a reagent-less protein assaying capability *if* the redox transducer is suitably coupled and cleanly analysed.[32] Open circuit potential (OCP) analyses are electronically and chemically simple (a direct, non-sandwich, platform) and unusually benign (the measurement itself occurs with zero current flow between working and counter electrodes; the circuitry is low cost and easily scaled).[33] They have been applied to the monitoring of oxidase activity (and thus glucose substrate) at glucose oxidase modified electrodes,[34] and to assess enzyme turnover kinetics in the presence of redox mediators.[33] Previous attempts to assay biomarkers by OCP have been limited to a low signal/noise (even after the application of an amplifying circuit) FET configuration or the use of an amplifying secondary labelling procedure.[35–37] To the best of our knowledge, there has been no prior application to any real time analysis of protein recognition.

The facile integration of electrochemical sensors into microfluidic formats can underpin assay automation at markedly reduced sample volumes,[38] and a myriad of microfluidic electrochemical sensors have been reported that are capable of the quantification of proteins, nucleic acids, pathogens, small molecules, and other target analytes.[39] The synergistic effect of integrating microfluidics with electrochemical techniques provided users with precise control on the flow of samples and reagents in a predetermined pattern. This has allowed the introduction of multi-functional diagnostic platforms capable of performing target extraction, pre-concentration, lysis, or coupling to secondary

probes.[40,41] Notably, microfluidic systems offer improved mass transport (as result of the combined effects of increased surface area:volume and continuous controllable convection)[40] and thus helpfully eat into the typically long incubation times often required within more conventional formats.[42,43] The use of 3D printing as a tool for microfluidic fabrication has dramatically boosted its flexibility and availability, offering a low-cost prototyping and construction strategy that can be applied to a number of assay types.[44]

Herein we integrate OCP measurements into a continuous flow 3D printed microfluidic system (Scheme 1, Figure S1, SI) in enabling a real-time assessment of antibody-antigen interactions at a working electrode surface. The concentration-dependent changes not only support a realistic biomarker quantification platform in a complex matrix but also enable protein: protein interaction kinetics to be extracted at low cost.

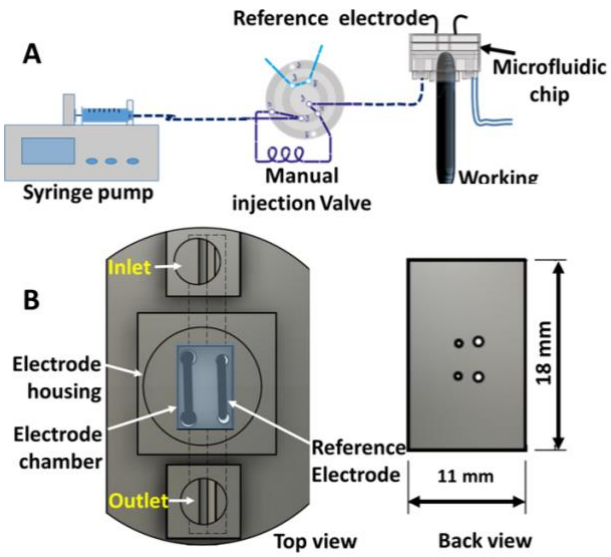

Scheme 1: Schematic representation of the microfluidic configuration designed to house conventional 6.4 mm disk electrodes with 2-3 mm working electrode diameter along with a home-made Nafion-coated Ag/AgCl reference electrode. (A) The system comprises an infusion syringe pump to precisely control running electrolyte flow rate, connected to a manual injection valve for the introduction of specific sample volumes. (B) Detailed depiction of the microfluidic chip featuring an electrode housing chamber (3 X 2 X 4.5 mm) that squarely sit on top of the working disk electrode and integrates a 0.7 mm diameter home-made reference Ag/AgCl electrode coated with a thin layer of Nafion. This chamber is connected to an inlet and outlet for delivery and disposal of running solution and samples.

Results and discussion

We start by considering an electrolyte-immersed receptor-modified electrode as a single plate of a parallel-plate capacitor, with the electrolyte solution comprising the second plate sandwiching a dielectric biolayer (Figure 1). Within the normal picture of a thin dielectric of length (d) across a

surface area (A). In order to simplify the model, we assume a uniform charge distribution on each plate. Under these conditions the electric field (E) is given by:[45,46]

$$E = \frac{Q}{\varepsilon.A} \qquad \text{Equation 1}$$

Where Q is the charge on each plate and Ɛ the dielectric permittivity. Under open circuit conditions (negligible current flow between working and counter electrode), the potential difference drop between the two capacitor plates is the OCP and is equal to the line integral of electric field (E) in the *z* direction from one plate to the other as approximated by equation 2.[47]

$$V_{OCP} = \int_0^d E(z)dz = Ed = \frac{Q.d}{\varepsilon.A} \qquad \text{Equation 2}$$

In the normal limit of electrode A>>d, recognition induced changes in V_{OCP} arise from perturbations of dielectric permittivity.[48,49] These perturbations are translated directly as a potential difference between working and reference electrodes measured using a potentiostat (in this case functioning as a voltmeter with negligible / femto-ampere range current).[31] To investigate the applicability of the system as a tool for reagent-less label-free protein quantitation, increasing concentrations of CRP spiked in 5% fetal bovine serum (FBS) (as a surrogate for a protein-rich matrix) were tested (Figure 1). The measurements were performed on both glassy carbon electrode (GCE) and gold working electrodes (Au electrode) modified with a composite receptive antibody and backfilled BSA film (through a standard physisorption protocol).[50] Figure 2A shows representative OCP dose-response curve for CRP (Figure S2, SI). The flow-based microfluidic configuration provides a precise control on electrolyte composition in the electrode chamber at any given time with a highly stable baseline (less than 1% SD over 100 min (Figure S3, SI). OCP changes respond to injection/change in solution dielectric (Figure 2A) and are thereafter stable (within 5 mV) prior to a specific recognition event.

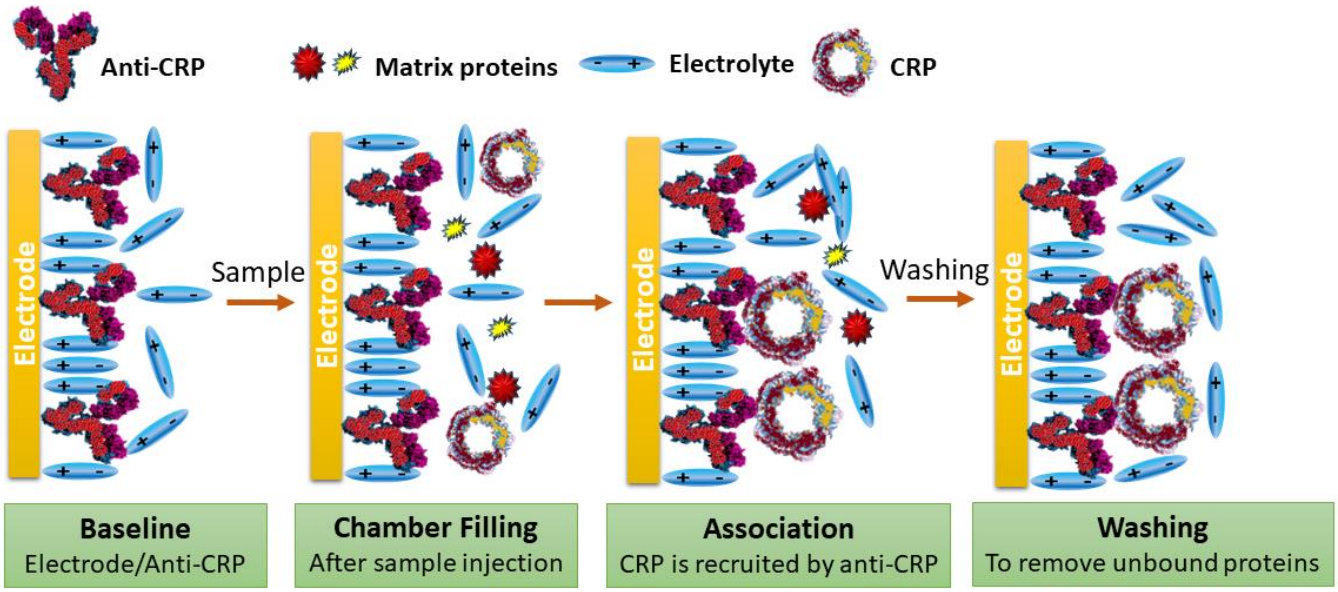

Figure 1: (A) Schematic depiction of the receptive electrode interface and the changes associated with sample injection, binding, and subsequent washing and equilibration. Target induced perturbations at the electrode-confined receptor antibody layer result in a detectable change in film dielectric.

Results presented in Figure 2B and 2C show that, while the value of the initial OCP is dependent on the nature of the working electrode (-50 ± 10 mV for bare GCE Vs -15 ± 5 mV for bare gold disk electrodes), values stabilize (less than 5 mV change over 400s) at very comparable magnitudes after blocking electrodes with 1 % BSA in 1M ethanolamine/ PBS (-5 ± 1 mV for both GCE and Au electrode). Subsequent manual sample injection produces a transitory fluctuation in the flow rate and bulk solution composition resulting in a temporary baseline perturbation (commonly encountered in flow-based assays),[51,52] that subsequently re-stabilises (Figure 2A and Figure S2, SI). Injected protein concentrations were calculated from the difference in the mean baseline OCP values (averaged for 100s) before and after sample injection (as indicated by black arrows in Figure 2A). For each concentration, OCP was recorded 20-30 minutes after each injection over a 100s period to confirm that all non-bound species are washed from the electrode surface and measured OCP changes thereafter reflective of captured target (as indicated by the stable OCP baseline (see for example Figure S3). An OCP signal with standard deviation (SD) <1% over this period was taken to represent the baseline; negligible OCP changes were observed thereafter (as indicated in figure S3, SI showing baseline stability study over a 100 *min* period). For subsequent quantifications, OCP measurements were again averaged over 100s after baseline stabilization for each sample injection. For triplicate measurements, standard deviations were calculated across the 3 independent measurements over 300s, cumulatively. Both Au and carbon

receptive interfaces exhibit target induced responses that are comparable in magnitude with concentrations (rather than the sequential concentration increments (serial additions) as

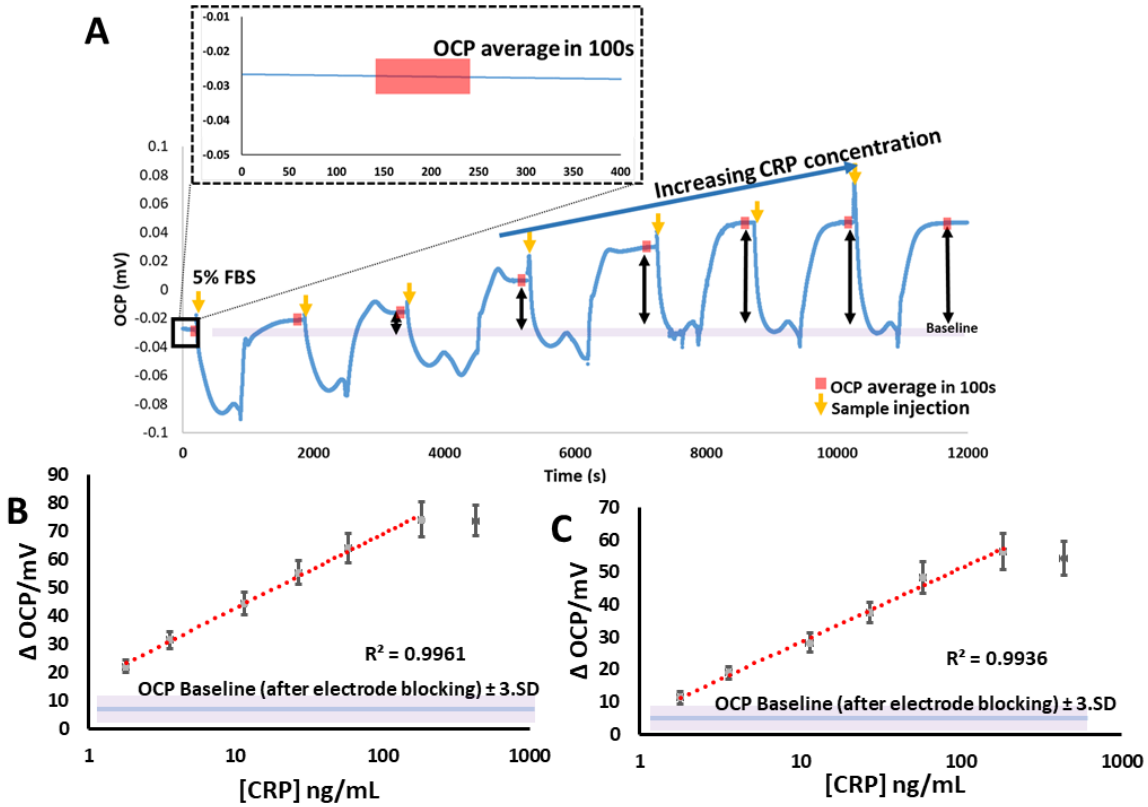

detection limits of 1ng/mL CRP in 5% FBS (in PBS) (Blank + 3 xSD calculated over 300s from 3 independent measurements (100s/trial)) and a >2 orders dynamic range (2-300 ng/mL). The difference in OCP before and after sample injection (black arrows, Figure 2) was correlated to target CRP concentration. Standard deviations for any given CRP concentration across triplicate measurements on 3 independent electrodes were <10 %. Gold interfaces were observed to yield a consistently higher (10-20%) analytical sensitivity (11-12 mV/log [CRP] ng/mL vs 9-10 mV/log [CRP] ng/mL). Analytical performance was further examined by exposing anti-CRP modified electrodes to random (non-serial) CRP shown Figure S4, SI. Responses show a dose-dependent response regardless of injection sequence (Figure S4, SI). The nature and concentration of the electrolyte solution was optimized to achieve minimal background noise with maximal signal/noise. A range of electrolytes (sodium chloride, potassium chloride, potassium nitrate, along with sodium ascorbate) were initially tested and sodium ascorbate found to produce the most stable baselines (less than 5 mV change over 10 min). 0.1 M Na-Asc was thereafter applied as the running electrolyte.

Figure 2: (A) Representative temporal response of a receptive gold working electrode observed during injection of increasing concentrations of CRP spiked into 5% FBS (in PBS). The inset shows baseline stability over 400s. OCP values corresponding to each concentration were taken from the mean of a 100s stable baseline (as indicated by the red boxes). Representative dose-response of gold disk and carbon electrodes (B and C, respectively). The red dotted line is the fitted linear correlation with its associated regression coefficient. The indicated baseline corresponds to the stable OCP at the modified electrode ± (3 X standard deviation (SD) in running buffer prior to sample injection. Error bars represent standard deviations from 3 independent measurements for each concentration.

Specificity and Analytical Validation OCP baseline stability was challenged by injecting successive volumes of protein-free PBS buffer and shows extremely low temporal drift (less than 5 mV over 6000s), without significant change upon injecting a protein rich 5% FBS (in PBS) matrix (Figure S5, SI). In order to further assess the specificity of the measured OCP response, electrodes were exposed to high, and clinically relevant, concentrations of interfering proteins (human serum albumin (HSA), fibrinogen, bovine serum albumin (BSA), and myoglobin) and 5% human serum in PBS. Responses to all were within background noise (± 5 mV); markedly below the response corresponding to the CRP LOD of 1ng/mL) (Figure S6, SI) indicating an excellent level of assay specificity at a chemically simple interface (Figure 3). This further highlights the beneficial effects of microfluidic continuous flow in reducing nonspecific adsorption and improving both signal/noise and assay sensitivity.[53,54] Further validation was then carried out in spiked human serum with recoveries in the 85-115% range (Figure 4) well within the acceptable limits for a ligand binding assays (80-120% recoveries) (Figure 4).[55] The baseline human serum CRP level was resolved as 2.3 ng/mL i.e. well below the normal range (baseline <3.0 µg/mL with increases up to 200 µg/mL after myocardial infarction).[56] Sensor regeneration is achieved by exposure to glycine-HCl buffer (pH 3.0; Figure S7, SI) the sensors lose ~ 10% activity after first regeneration cycle with subsequent antigen response reduced to 70% of the original, observations that are indicative of a need for further optimization but in line with previous reports.[57,58]

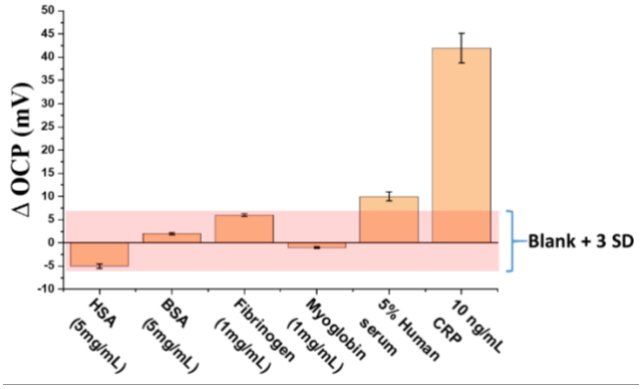

Figure 3: OCP response as a function of challenging a typical gold sensor to common interfering proteins. Columns represent OCP magnitude changes at equilibrium in 0.1 M Na-Asc flowing at 20 µL/min before and after injecting each sample. Error bars represent standard deviations from 3 independent measurements for each sample.

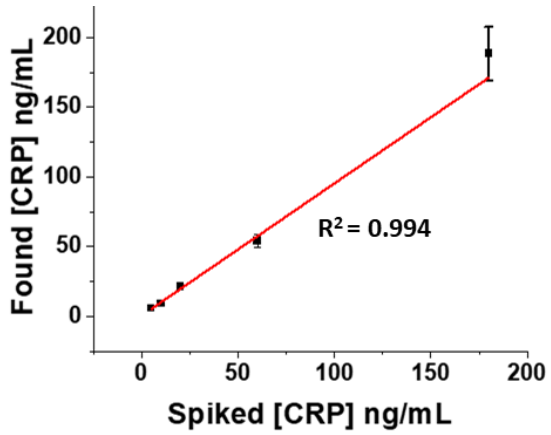

Spiked [CRP] ng/mL	Found [CRP] ng/mL	Percent Recovery (%)	Percent Standard deviation (%)
5.00	5.21	104.20	7.87
10.0	9.34	93.41	7.92
20.0	22.54	112.72	8.16
60.0	53.21	88.68	9.36
180	189.3	105.13	7.51

Figure 4: Correlation between actual spiked and assay resolved CRP concentration. Correlation coefficients found/spiked and slope were close to unity (0.994 and 0.947, respectively) indicating an excellent correlation. Assay data here from gold sensors with "found" concentrations estimated from dose-response calibrations (Figure 2) after subtracting background (in 5% human serum in PBS). Standard deviations across 3 independent repeats were less than 10%. Error bars represent standard deviations from 3 independent measurements.

Kinetic analysis Since the interaction of the target protein and electrode confined antibodies can be resolved in real-time, we hypothesized an ability to resolve binding and dissociation kinetics. Under a constant injected flow rate (20 µL/min), temporal OCP changes (after CRP samples reach the electrode chamber, some 5 minutes after injection) were well described by a simple 1: 1 binding model from which apparent association and dissociation rate constants (k_a and k_d, respectively) and thermodynamic dissociation constants, K_D ($= \frac{k_d}{k_a}$) can be estimated using equation 3 and 4.[59]

$$V_{OCP} = C.k_a.V_{OCP\,max}\frac{\{1 - \exp[-(C.k_a + k_d).t]\}}{C.k_a + k_d} \qquad \text{(Equation 3)}$$

$$V_{OCP} = V_{OCP\,max}.\ \exp(-k_d.t) \qquad \text{(Equation 4)}$$

Here V_{OCP} corresponds to OCP magnitude at time t, C the CRP bulk concentration, and $V_{OCP\,max}$ the maximum OCP response. Apparent association and dissociation rate constants across a range of marker concentrations (Figure 5) were calculated after a fitting of their corresponding OCP data using Origin software. The apparent dissociation constant calculated using equation 3 was 1.50±0.20 nM in excellent agreement with that determined by SPR at an equivalently prepared gold SPR interface (1.28 nM) (Figure S8, SI).

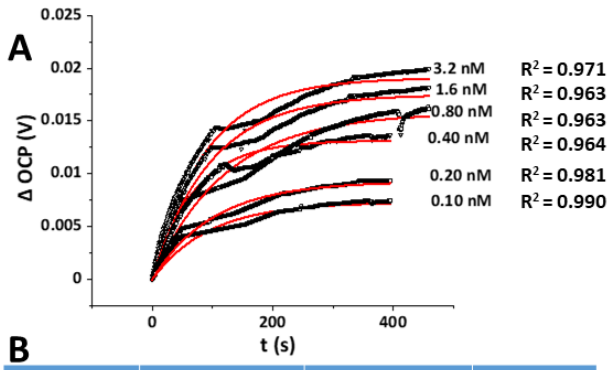

B

CRP concentration (nM)	Association rate constant, k_a ($M^{-1} s^{-1}$)	Dissociation rate constant, k_d (s^{-1})	Dissociation constant, K_D (nM)
0.1	$2.16 \pm 0.03 \times 10^5$	$3.61 \pm 0.02 \times 10^{-4}$	1.66
0.2	$2.57 \pm 0.04 \times 10^5$	$4.31 \pm 0.01 \times 10^{-4}$	1.68
0.40	$3.87 \pm 0.05 \times 10^5$	$4.77 \pm 0.05 \times 10^{-4}$	1.23
0.80	$3.42 \pm 0.04 \times 10^5$	$5.49 \pm 0.05 \times 10^{-4}$	1.61
1.60	$3.47 \pm 0.04 \times 10^5$	$5.79 \pm 0.05 \times 10^{-4}$	1.67
3.20	$3.66 \pm 0.05 \times 10^5$	$5.35 \pm 0.05 \times 10^{-4}$	1.47

Figure 5: (A) Real time OCP measurements in the presence of specific CRP concentrations at receptor modified gold sensors in 0.1 M sodium ascorbate at 20 µL/min (black lines). Nonlinear regression fittings using equation 3 and 4 (red lines) are shown (regression coefficients between 0.963 and 0.990). (B) Apparent association and dissociation rate constants resolved from OCP measurements (standard deviations less than 10 %).

The results herein demonstrate the utilization of simple real-time OCP assessments in quantifying the kinetics, thermodynamics and target concentration of a model protein biomarker (CRP). Assays were performed within custom made, printed, flow cells at conventional working electrodes. OCP assessments are, almost by definition, benign and require no secondary target labelling or subsequent amplification steps. They are of considerable potential value in translating a detection capability to a low cost, scaleable format. The ability to resolve well-defined association and dissociation events facilitates a robust analysis of binding kinetics within a format that additionally allows specific target quantification with good selectivity in complex matrices like serum. The simplicity and sensitivity of the platform is relevant not only to potential "point of care" application but also as a means of cross-validating optical or computational modelling, or (with ultra-micro electrodes) *in vivo* or intracellular assays/kinetic analyses.[60,61]

Clinical Assessment of patient samples A duplicate analysis of 7 samples from a local hospital (Table S1, SI) showed an excellent correlation with ELISA (Figure 6). CRP levels as quantified through OCP analysis showed an excellent correlation with reported immunoassay results (<15% difference in the mean). The correlation between the two sets showed a slope close to unity (0.098) and intercept close to zero (0.025) indicating a good agreement between the two analyses. A paired t-test (at 95% confidence interval) resolves a value of 0.24 (> 0.05) indicating no significant different between the two assay results.[62]

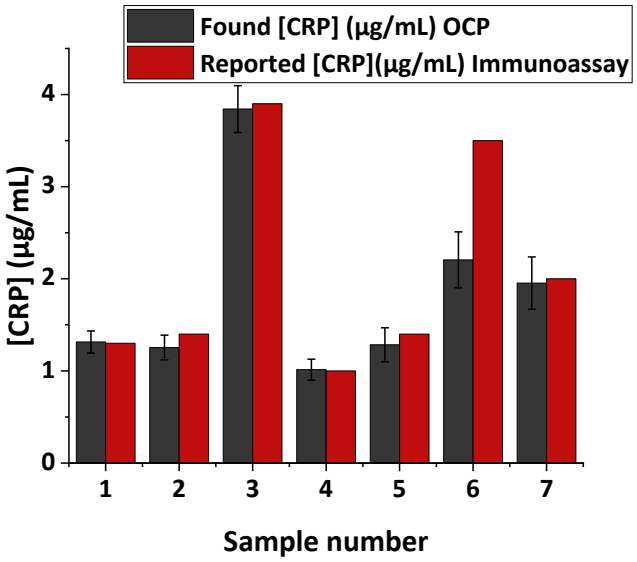

Figure 6: A bar chart comparison of CRP concentrations resolved by OCP and ELISA. Error bars represent standard deviations in two independent measurements. There is one outlier (Patient 6) but otherwise analyses show an alignment that is in the 85-115% range, excellent for real sample analysis by two independent methods.

Conclusion

Herein an OCP-based platform for protein quantification at simple, receptor modified, electrodes, is reported. Biomarker assay times are less than 20 minutes, sensitive, and entirely reagentless. CRP assays showed excellent recoveries from spiked human serum samples with minimal matrix effect. Temporal association/dissociation patterns were well-resolved, fitted to a standard 1:1 binding model, and used to accurately assess binding kinetics.

Materials

Gold and glassy carbon working disk electrodes were from CHI (TX, USA) with geometrical conductive diameter of 2-3 mm. Silver and platinum wires were purchased from Advent research and materials (Witney, UK). Sodium ascorbate, phosphate buffer saline tablets, sulfuric acid and potassium hydroxide were of analytical grade from Sigma Aldrich. Native human C-reactive protein (CRP) (Cat#1707) and goat polyclonal anti-human CRP antibodies (Anti-CRP) were from Bio-Rad Laboratories Inc. All electrochemical measurements were performed using a portable PalmSens4 potentiostat controlled by PSTrace 5.8 software (PalmSens BV, The Netherlands).

Electrode antibody functionalization Gold disk electrodes were polished sequentially with 1.0 µm, 0.3 µm, and 0.05 µm alumina and cleaned with Piranha solution for 5 min. Electrodes were then cycled in 0.5 M sulfuric acid between -0.15 and 1.35 V Vs Ag/AgCl reference electrode at 100 mV/s for 100 cycles. Electrodes were then incubated with a solution of 100 µg/mL of Ab in PBS at pH 7.4 for at least 16h at 4°C. Glassy carbon working disk electrodes were polished sequentially with 1.0 µm, 0.3 µm, and 0.05 µm alumina, and cycled in 0.5 M potassium hydroxide between 0.70 and 1.70V Vs Ag/AgCl reference electrode at 100 mV/s for 10 cycles. They were then incubated for 16h with 100 µg/mL of Ab at 4°C.

Microfluidic sample handling A microfluidic chip was custom designed to precisely handle the delivery, incubation and wash of samples and electrolyte solution into a ≈ 30 µL chamber squarely accommodating 2-3 mm diameter working disk electrodes (WE). The chip was integrated into a continuous flow system controlled by a positive infusion syringe pump (PHD 22/2000, Harvard Apparatus®) connected to a manual sample injection valve (Rheodyne® Model 7125 Injector) with 100 µL sample loop. The electrode chamber is equipped with a home-made reference Ag/AgCl (coated with 5 layers of Nafion®117 (Sigma Aldrich) to forma a protective membrane to reduce leaching) and counter platinum wire electrodes for electrochemical measurements. First, 0.1 M sodium ascorbate (Na-Asc) in infused at a flow rate of 50 µL/min and open circuit potential (OCP) is monitored. Samples are then loaded into the 100 µL sample loop, with the injection valve switched into injection mode. Based on to the cross dimensions and length of the connecting tubing, 120s are required to fill the electrode chamber. Flow is then changed to 10 µL/min for 10 min to facilitate target protein capture. Unbound species are then washed by flowing 0.1 M Na-Asc at 200 µL/min for 1 min, prior to flow being switched back to 50 µL/min until the next sample injection. All samples were diluted in PBS buffer pH 7.4 to resemble serum pH. 5% FBS was prepared by diluting fetal bovine serum (Sigma Aldrich) in PBS buffer, and human serum (Sigma Aldrich) was diluted in PBS (pH 7.4). Blocking buffer was 1 % bovine serum albumin (Sigma Aldrich) in 0.1 M ethanolamine in PBS (pH 7.4).

Sensor regeneration and reusability electrodes with Anti-CRP were first exposed to a CRP sample of 10 ng/mL, followed by running electrolyte for 10 min at 50 µL/min. Electrodes were then washed with 10 mM glycine/HCl buffer (pH 3.0) to remove bound antigen for 2 min.

SPR kinetic and affinity studies of Anti-CRP anti-CRP antibodies were physisorbed on gold SPR chip, inserted in Biacore X-100 SPR under running PBS buffer. A series of five CRP concentrations were injected sequentially without washing while recording SPR intensities. Association and dissociation rate constants were determined by global fitting of the data using the 1 : 1 Langmuir binding model; dissociation constant (K_D) was calculated from the ratio of the dissociation rate constant to association rate constant (k_d/k_a).

Patients Samples analysis 7 Patient Samples supplied by John Radcliffe (JR) Hospital (Oxford University Hospitals) were analyzed in duplicate. Samples were thawed upon receipt, aliquoted into 5µL batches, and stored at -80° C. One hundred-fold dilutions were carried out just prior to use to bring CRP concentrations into the assay dynamic range, then 100 µL volumes injected using the

sample injection loop. OCP was measured in running electrolyte solution of 0.1 M sodium ascorbate.

Notes

M.S. declares no competing financial interests. J.J.D. is a founder of Osler Diagnostics. Osler Diagnostics are developing electrochemical diagnostic devices.

Supporting Information: Microfluidic system for real-time OCP measurement; Real-time OCP Sensorgram; OCP baseline stability; OCP calibration with random OCP injections; Baseline stability and assay specificity; Assay specificity; Sensor regeneration; SPR kinetic and affinity studies of Anti-CRP; Patient samples Analysis.

Acknowledgements

The authors thank Osler Diagnostics for support.

References

(1) Giljohann, D. A.; Mirkin, C. A. Drivers of Biodiagnostic Development. *Nature* **2009**, *462* (7272), 461–464. https://doi.org/10.1038/nature08605.

(2) Goossens, N.; Nakagawa, S.; Sun, X.; Hoshida, Y. Cancer Biomarker Discovery and Validation. *Transl Cancer Res* **2015**, *4* (3), 256–269. https://doi.org/10.3978/j.issn.2218-676X.2015.06.04.

(3) Harris, S. E.; Cox, S. R.; Bell, S.; Marioni, R. E.; Prins, B. P.; Pattie, A.; Corley, J.; Muñoz Maniega, S.; Valdés Hernández, M.; Morris, Z.; John, S.; Bronson, P. G.; Tucker-Drob, E. M.; Starr, J. M.; Bastin, M. E.; Wardlaw, J. M.; Butterworth, A. S.; Deary, I. J. Neurology-Related Protein Biomarkers Are Associated with Cognitive Ability and Brain Volume in Older Age. *Nature Communications* **2020**, *11* (1), 800. https://doi.org/10.1038/s41467-019-14161-7.

(4) Bing, R.; Henderson, J.; Hunter, A.; Williams, M. C.; Moss, A. J.; Shah, A. S. V.; McAllister, D. A.; Dweck, M. R.; Newby, D. E.; Mills, N. L.; Adamson, P. D. Clinical Determinants of Plasma Cardiac Biomarkers in Patients with Stable Chest Pain. *Heart* **2019**, *105* (22), 1748–1754. https://doi.org/10.1136/heartjnl-2019-314892.

(5) Hirata, T.; Arai, Y.; Yuasa, S.; Abe, Y.; Takayama, M.; Sasaki, T.; Kunitomi, A.; Inagaki, H.; Endo, M.; Morinaga, J.; Yoshimura, K.; Adachi, T.; Oike, Y.; Takebayashi, T.; Okano, H.; Hirose, N. Associations of Cardiovascular Biomarkers and Plasma Albumin with Exceptional Survival to the Highest Ages. *Nature Communications* **2020**, *11* (1), 3820. https://doi.org/10.1038/s41467-020-17636-0.

(6) Sharafeldin, M.; Davis, J. J. Point of Care Sensors for Infectious Pathogens. *Anal. Chem.* **2021**, *93* (1), 184–197. https://doi.org/10.1021/acs.analchem.0c04677.

(7) Mintz, A.; Gibo, D. M.; MadhanKumar, A. B.; Cladel, N. M.; Christensen, N. D.; Debinski, W. Protein- and DNA-Based Active Immunotherapy Targeting Interleukin-13 Receptor Alpha2. *Cancer Biother Radiopharm* **2008**, *23* (5), 581–589. https://doi.org/10.1089/cbr.2008.0462.

(8) Lu, H.; Zhou, Q.; He, J.; Jiang, Z.; Peng, C.; Tong, R.; Shi, J. Recent Advances in the Development of Protein–Protein Interactions Modulators: Mechanisms and Clinical Trials. *Signal Transduction and Targeted Therapy* **2020**, *5* (1), 1–23. https://doi.org/10.1038/s41392-020-00315-3.

(9) Ruffalo, M.; Bar-Joseph, Z. Protein Interaction Disruption in Cancer. *BMC Cancer* **2019**, *19* (1), 370. https://doi.org/10.1186/s12885-019-5532-5.

(10) Singh, P.; Roche, A.; van der Walle, C. F.; Uddin, S.; Du, J.; Warwicker, J.; Pluen, A.; Curtis, R. Determination of Protein–Protein Interactions in a Mixture of Two Monoclonal Antibodies. *Mol. Pharmaceutics* **2019**, *16* (12), 4775–4786. https://doi.org/10.1021/acs.molpharmaceut.9b00430.

(11) Pérez-Ruiz, E.; Decrop, D.; Ven, K.; Tripodi, L.; Leirs, K.; Rosseels, J.; van de Wouwer, M.; Geukens, N.; De Vos, A.; Vanmechelen, E.; Winderickx, J.; Lammertyn, J.; Spasic, D. Digital ELISA for the Quantification of Attomolar Concentrations of Alzheimer's Disease Biomarker Protein Tau in Biological Samples. *Analytica Chimica Acta* **2018**, *1015*, 74–81. https://doi.org/10.1016/j.aca.2018.02.011.

(12) Tan, X.; Chen, Q.; Zhu, H.; Zhu, S.; Gong, Y.; Wu, X.; Chen, Y.-C.; Li, X.; Li, M. W.-H.; Liu, W.; Fan, X. Fast and Reproducible ELISA Laser Platform for Ultrasensitive Protein Quantification. *ACS Sens.* **2020**, *5* (1), 110–117. https://doi.org/10.1021/acssensors.9b01795.

(13) Douzi, B. Protein–Protein Interactions: Surface Plasmon Resonance. In *Bacterial Protein Secretion Systems: Methods and Protocols*; Journet, L., Cascales, E., Eds.; Methods in Molecular Biology; Springer: New York, NY, 2017; pp 257–275. https://doi.org/10.1007/978-1-4939-7033-9_21.

(14) Goldring, J. P. D. Protein Quantification Methods to Determine Protein Concentration Prior to Electrophoresis. In *Protein Electrophoresis: Methods and Protocols*; Kurien, B. T., Scofield, R. H., Eds.; Methods in Molecular Biology; Humana Press: Totowa, NJ, 2012; pp 29–35. https://doi.org/10.1007/978-1-61779-821-4_3.

(15) Pan, S.; Aebersold, R.; Chen, R.; Rush, J.; Goodlett, D. R.; McIntosh, M. W.; Zhang, J.; Brentnall, T. A. Mass Spectrometry Based Targeted Protein Quantification: Methods and Applications. *J. Proteome Res.* **2009**, *8* (2), 787–797. https://doi.org/10.1021/pr800538n.

(16) Velazquez-Campoy, A.; Leavitt, S. A.; Freire, E. Characterization of Protein-Protein Interactions by Isothermal Titration Calorimetry. *Methods Mol Biol* **2015**, *1278*, 183–204. https://doi.org/10.1007/978-1-4939-2425-7_11.

(17) Gonzalez, L. C. Protein Microarrays, Biosensors, and Cell-Based Methods for Secretome-Wide Extracellular Protein–Protein Interaction Mapping. *Methods* **2012**, *57* (4), 448–458. https://doi.org/10.1016/j.ymeth.2012.06.004.

(18) Ronkainen-Matsuno, N. J.; Thomas, J. H.; Halsall, H. B.; Heineman, W. R. Electrochemical Immunoassay Moving into the Fast Lane. *TrAC Trends in Analytical Chemistry* **2002**, *21* (4), 213–225. https://doi.org/10.1016/S0165-9936(02)00401-6.

(19) Ibáñez-Redín, G.; Joshi, N.; do Nascimento, G. F.; Wilson, D.; Melendez, M. E.; Carvalho, A. L.; Reis, R. M.; Gonçalves, D.; Oliveira, O. N. Determination of P53 Biomarker Using an Electrochemical Immunoassay Based on Layer-by-Layer Films with NiFe2O4 Nanoparticles. *Microchim Acta* **2020**, *187* (11), 619. https://doi.org/10.1007/s00604-020-04594-z.

(20) Viswanathan, S.; Narayanan, T. N.; Aran, K.; Fink, K. D.; Paredes, J.; Ajayan, P. M.; Filipek, S.; Miszta, P.; Tekin, H. C.; Inci, F.; Demirci, U.; Li, P.; Bolotin, K. I.; Liepmann, D.; Renugopalakrishanan, V. Graphene–Protein Field Effect Biosensors: Glucose Sensing. *Materials Today* **2015**, *18* (9), 513–522.

https://doi.org/10.1016/j.mattod.2015.04.003.

(21) Lin, P.-H.; Li, B.-R. Antifouling Strategies in Advanced Electrochemical Sensors and Biosensors. *Analyst* **2020**, *145* (4), 1110–1120. https://doi.org/10.1039/C9AN02017A.

(22) Kumar, S.; Bukkitgar, S. D.; Singh, S.; Pratibha; Singh, V.; Reddy, K. R.; Shetti, N. P.; Reddy, C. V.; Sadhu, V.; Naveen, S. Electrochemical Sensors and Biosensors Based on Graphene Functionalized with Metal Oxide Nanostructures for Healthcare Applications. *ChemistrySelect* **2019**, *4* (18), 5322–5337. https://doi.org/10.1002/slct.201803871.

(23) Lin, M.; Song, P.; Zhou, G.; Zuo, X.; Aldalbahi, A.; Lou, X.; Shi, J.; Fan, C. Electrochemical Detection of Nucleic Acids, Proteins, Small Molecules and Cells Using a DNA-Nanostructure-Based Universal Biosensing Platform. *Nature Protocols* **2016**, *11* (7), 1244–1263. https://doi.org/10.1038/nprot.2016.071.

(24) Mahshid, S. S.; Mahshid, S.; Vallée-Bélisle, A.; Kelley, S. O. Peptide-Mediated Electrochemical Steric Hindrance Assay for One-Step Detection of HIV Antibodies. *Anal. Chem.* **2019**, *91* (8), 4943–4947. https://doi.org/10.1021/acs.analchem.9b00648.

(25) Wei, R.; Gatterdam, V.; Wieneke, R.; Tampé, R.; Rant, U. Stochastic Sensing of Proteins with Receptor-Modified Solid-State Nanopores. *Nature Nanotechnology* **2012**, *7* (4), 257–263. https://doi.org/10.1038/nnano.2012.24.

(26) Ying, Y.-L.; Yu, R.-J.; Hu, Y.-X.; Gao, R.; Long, Y.-T. Single Antibody–Antigen Interactions Monitored via Transient Ionic Current Recording Using Nanopore Sensors. *Chemical Communications* **2017**, *53* (61), 8620–8623. https://doi.org/10.1039/C7CC03927A.

(27) Thakur, A. K.; Movileanu, L. Real-Time Measurement of Protein–Protein Interactions at Single-Molecule Resolution Using a Biological Nanopore. *Nature Biotechnology* **2019**, *37* (1), 96–101. https://doi.org/10.1038/nbt.4316.

(28) Boon, E. M.; Salas, J. E.; Barton, J. K. An Electrical Probe of Protein–DNA Interactions on DNA-Modified Surfaces. *Nature Biotechnology* **2002**, *20* (3), 282–286. https://doi.org/10.1038/nbt0302-282.

(29) Das, J.; Gomis, S.; Chen, J. B.; Yousefi, H.; Ahmed, S.; Mahmud, A.; Zhou, W.; Sargent, E. H.; Kelley, S. O. Reagentless Biomolecular Analysis Using a Molecular Pendulum. *Nat. Chem.* **2021**, 1–7. https://doi.org/10.1038/s41557-021-00644-y.

(30) Yousefi, H.; Mahmud, A.; Chang, D.; Das, J.; Gomis, S.; Chen, J. B.; Wang, H.; Been, T.; Yip, L.; Coomes, E.; Li, Z.; Mubareka, S.; McGeer, A.; Christie, N.; Gray-Owen, S.; Cochrane, A.; Rini, J. M.; Sargent, E. H.; Kelley, S. O. Detection of SARS-CoV-2 Viral Particles Using Direct, Reagent-Free Electrochemical Sensing. *J. Am. Chem. Soc.* **2021**, *143* (4), 1722–1727. https://doi.org/10.1021/jacs.0c10810.

(31) Kanyong, P.; Patil, A. V.; Davis, J. J. Functional Molecular Interfaces for Impedance-Based Diagnostics. *Annual Review of Analytical Chemistry* **2020**, *13* (1), 183–200. https://doi.org/10.1146/annurev-anchem-061318-115600.

(32) Bueno, P. R.; Fernandes, F. C. B.; Davis, J. J. Quantum Capacitance as a Reagentless Molecular Sensing Element. *Nanoscale* **2017**, *9* (40), 15362–15370. https://doi.org/10.1039/C7NR06160A.

(33) Smith, L. A.; Glasscott, M. W.; Vannoy, K. J.; Dick, J. E. Enzyme Kinetics via Open Circuit Potentiometry. *Anal. Chem.* **2020**, *92* (2), 2266–2273. https://doi.org/10.1021/acs.analchem.9b04972.

(34) Song, Y.; Su, D.; Shen, Y.; Liu, H.; Wang, L. Design and Preparation of Open Circuit Potential Biosensor for in Vitro and in Vivo Glucose Monitoring. *Anal Bioanal Chem*

2017, *409* (1), 161–168. https://doi.org/10.1007/s00216-016-9982-1.

(35) Charoenkitamorn, K.; Tue, P. T.; Kawai, K.; Chailapakul, O.; Takamura, Y. Electrochemical Immunoassay Using Open Circuit Potential Detection Labeled by Platinum Nanoparticles. *Sensors* **2018**, *18* (2), 444. https://doi.org/10.3390/s18020444.

(36) Wong, L. C. C.; Jolly, P.; Estrela, P. Development of a Sensitive Multiplexed Open Circuit Potential System for the Detection of Prostate Cancer Biomarkers. *BioNanoSci.* **2018**, *8* (2), 701–706. https://doi.org/10.1007/s12668-017-0408-0.

(37) Estrela, P.; Paul, D.; Li, P.; Keighley, S. D.; Migliorato, P.; Laurenson, S.; Ferrigno, P. K. Label-Free Detection of Protein Interactions with Peptide Aptamers by Open Circuit Potential Measurement. *Electrochimica Acta* **2008**, *53* (22), 6489–6496. https://doi.org/10.1016/j.electacta.2008.04.036.

(38) Fernández-la-Villa, A.; Pozo-Ayuso, D. F.; Castaño-Álvarez, M. Microfluidics and Electrochemistry: An Emerging Tandem for next-Generation Analytical Microsystems. *Current Opinion in Electrochemistry* **2019**, *15*, 175–185. https://doi.org/10.1016/j.coelec.2019.05.014.

(39) Nesakumar, N.; Kesavan, S.; Li, C.-Z.; Alwarappan, S. Microfluidic Electrochemical Devices for Biosensing. *J. Anal. Test.* **2019**, *3* (1), 3–18. https://doi.org/10.1007/s41664-019-0083-y.

(40) Sharafeldin, M.; Chen, T.; Ozkaya, G. U.; Choudhary, D.; Molinolo, A. A.; Gutkind, J. S.; Rusling, J. F. Detecting Cancer Metastasis and Accompanying Protein Biomarkers at Single Cell Levels Using a 3D-Printed Microfluidic Immunoarray. *Biosensors and Bioelectronics* **2021**, *171*, 112681. https://doi.org/10.1016/j.bios.2020.112681.

(41) Lin, J.-H.; Tsai, T.-T.; Zeng, Q.; Chang, C.-Y.; Guo, J.-Y.; Lin, C.-J.; Chen, C.-F. A Multifunctional Microfluidic Device for Blood Typing and Primary Screening of Blood Diseases. *ACS Sens.* **2020**, *5* (10), 3082–3090. https://doi.org/10.1021/acssensors.0c00969.

(42) Hervás, M.; López, M. A.; Escarpa, A. Electrochemical Immunosensing on Board Microfluidic Chip Platforms. *TrAC Trends in Analytical Chemistry* **2012**, *31*, 109–128. https://doi.org/10.1016/j.trac.2011.06.020.

(43) Nesakumar, N.; Kesavan, S.; Li, C.-Z.; Alwarappan, S. Microfluidic Electrochemical Devices for Biosensing. *J. Anal. Test.* **2019**, *3* (1), 3–18. https://doi.org/10.1007/s41664-019-0083-y.

(44) Sharafeldin, M.; Kadimisetty, K.; Bhalerao, K. S.; Chen, T.; Rusling, J. F. 3D-Printed Immunosensor Arrays for Cancer Diagnostics. *Sensors* **2020**, *20* (16), 4514. https://doi.org/10.3390/s20164514.

(45) Ellingson, S. W. *Electromagnetics, Volume 1*; VT Publishing, 2018. https://doi.org/10.21061/electromagnetics-vol-1.

(46) Wells, B.; Baker, E.; Farwell, A.; Foster, H.; Gao, X.; Gruber, B.; Jones, E.; Vu, D.; Xu, S.; Ye, J. An Adjustable Parallel-Plate Capacitor Instrument—Test of the Theoretical Capacitance Formula. *American Journal of Physics* **2016**, *84* (9), 723–726. https://doi.org/10.1119/1.4955143.

(47) Stanford, A. L.; Tanner, J. M. 14 - Capacitance, Current, and Resistance. In *Physics for Students of Science and Engineering*; Stanford, A. L., Tanner, J. M., Eds.; Academic Press, 1985; pp 394–423. https://doi.org/10.1016/B978-0-12-663380-1.50017-3.

(48) Li, L.; Li, C.; Zhang, Z.; Alexov, E. On the Dielectric "Constant" of Proteins: Smooth Dielectric Function for Macromolecular Modeling and Its Implementation in DelPhi. *J. Chem. Theory Comput.* **2013**, *9* (4), 2126–2136. https://doi.org/10.1021/ct400065j.

(49) Gebbert, Andreas.; Alvarez-Icaza, Manuel.; Stoecklein, Walter.; Schmid, R. D. Real-Time Monitoring of Immunochemical Interactions with a Tantalum Capacitance Flow-through Cell. *Anal. Chem.* **1992**, *64* (9), 997–1003. https://doi.org/10.1021/ac00033a007.

(50) Sharafeldin, M.; McCaffrey, K.; F. Rusling, J. Influence of Antibody Immobilization Strategy on Carbon Electrode Immunoarrays. *Analyst* **2019**, *144* (17), 5108–5116. https://doi.org/10.1039/C9AN01093A.

(51) Granqvist, N.; Hanning, A.; Eng, L.; Tuppurainen, J.; Viitala, T. Label-Enhanced Surface Plasmon Resonance: A New Concept for Improved Performance in Optical Biosensor Analysis. *Sensors (Basel)* **2013**, *13* (11), 15348–15363. https://doi.org/10.3390/s131115348.

(52) Schasfoort, R. B. M. Chapter 1:Introduction to Surface Plasmon Resonance. In *Handbook of Surface Plasmon Resonance*; 2017; pp 1–26. https://doi.org/10.1039/9781788010283-00001.

(53) Lichtenberg, J. Y.; Ling, Y.; Kim, S. Non-Specific Adsorption Reduction Methods in Biosensing. *Sensors* **2019**, *19* (11), 2488. https://doi.org/10.3390/s19112488.

(54) Bange, A.; Halsall, H. B.; Heineman, W. R. Microfluidic Immunosensor Systems. *Biosensors and Bioelectronics* **2005**, *20* (12), 2488–2503. https://doi.org/10.1016/j.bios.2004.10.016.

(55) Viswanathan, C. T.; Bansal, S.; Booth, B.; DeStefano, A. J.; Rose, M. J.; Sailstad, J.; Shah, V. P.; Skelly, J. P.; Swann, P. G.; Weiner, R. Quantitative Bioanalytical Methods Validation and Implementation: Best Practices for Chromatographic and Ligand Binding Assays. *Pharm Res* **2007**, *24* (10), 1962–1973. https://doi.org/10.1007/s11095-007-9291-7.

(56) Lagrand, W. K.; Visser, C. A.; Hermens, W. T.; Niessen, H. W. M.; Verheugt, F. W. A.; Wolbink, G.-J.; Hack, C. E. C-Reactive Protein as a Cardiovascular Risk Factor. *Circulation* **1999**, *100* (1), 96–102. https://doi.org/10.1161/01.CIR.100.1.96.

(57) Jeon, D.; Pyun, J.-C.; Jose, J.; Park, M. A Regenerative Immunoaffinity Layer Based on the Outer Membrane of Z-Domains Autodisplaying E. Coli for Immunoassays and Immunosensors. *Sensors* **2018**, *18* (11), 4030. https://doi.org/10.3390/s18114030.

(58) Wang, J.; Yao, W.; Meng, F.; Wang, P.; Wu, Y.; Wang, B. A Surface Plasmon Resonance Immunoassay for the Rapid Analysis of Methamphetamine in Forensic Oral Fluid. *Journal of Clinical Laboratory Analysis* **2019**, *33* (9), e22993. https://doi.org/10.1002/jcla.22993.

(59) Joshi, A. A.; Peczuh, M. W.; Kumar, C. V.; Rusling, J. F. Ultrasensitive Carbohydrate-Peptide SPR Imaging Microarray for Diagnosing IgE Mediated Peanut Allergy. *Analyst* **2014**, *139* (22), 5728–5733. https://doi.org/10.1039/C4AN01544D.

(60) Peng, X.; Wang, J.; Peng, W.; Wu, F.-X.; Pan, Y. Protein–Protein Interactions: Detection, Reliability Assessment and Applications. *Briefings in Bioinformatics* **2017**, *18* (5), 798–819. https://doi.org/10.1093/bib/bbw066.

(61) Xing, S.; Wallmeroth, N.; Berendzen, K. W.; Grefen, C. Techniques for the Analysis of Protein-Protein Interactions in Vivo1[OPEN]. *Plant Physiol* **2016**, *171* (2), 727–758. https://doi.org/10.1104/pp.16.00470.

(62) Rochon, J.; Gondan, M.; Kieser, M. To Test or Not to Test: Preliminary Assessment of Normality When Comparing Two Independent Samples. *BMC Medical*

Research Methodology **2012**, *12* (1), 81. https://doi.org/10.1186/1471-2288-12-81.

TOC

Open Circuit Potential (OCP) as a tool for the assessment of binding kinetics and reagentless protein quantitation

Mohamed Sharafeldin;[1] Tim James;[2] and Jason J. Davis[1]

[1] Department of Chemistry, University of Oxford, South Parks Road, Oxford OX1 3QZ, UK

[2] Department of Clinical Biochemistry, Oxford University Hospitals NHS Trust, Oxford, OX3 9DU, U.K.